A Novel Metric for mMIMO Base Station Association for Aerial Highway Systems

Matteo Bernabè*§, David López Pérez†, Nicola Piovesan*, Giovanni Geraci‡, and David Gesbert§

*Huawei Technologies, France †Univ. Politècnica de València, Spain ‡Univ. Pompeu Fabra, Spain §EURECOM, France

***Abstract*— In this article, we introduce a new metric for driving the serving cell selection process of a swarm of cellular connected unmanned aerial vehicles (CCUAVs) located on aerial highways when served by a massive multiple input multiple output (mMIMO) terrestrial network. Selecting the optimal serving cell from several suitable candidates is not straightforward. By solely relying on the traditional cell selection metric, based on reference signal received power (RSRP), it is possible to result in a scenario in which the serving cell can not multiplex an appropriate number of CCUAVs due to the high correlation in the line of sight (LoS) channels. To overcome such issue, in this work, we introduce a new cell selection metric to capture not only signal strength, but also spatial multiplexing capabilities. The proposed metric highly depends on the relative position between the aerial highways and the antennas of the base station. The numerical analysis indicates that the integration of the proposed new metric allows to have a better signal to interference plus noise ratio (SINR) performance on the aerial highways, resulting in a more reliable cellular connection for CCUAVs.**

I. Introduction

Remote piloted drones, also known as unmanned aerial vehicles (UAVs), have become increasingly important in recent years, having already had a major impact on different applications, such as surveillance and security, precision agriculture, and parcel delivery [1], [2]. In May 2021, Morgan Stanley predicted that, by 2050, the entire urban air mobility (UAM) market, including air taxis, delivery, and patrol drones, could reach a value up to $19 trillion, accounting for 10 to 11% of the projected United States global gross domestic product (GDP) [3]. In addition, it is expected that the intrinsic flexibility of UAVs will enable new disruptive industries and markets that are currently beyond our imagination.

The use of UAVs in communication networks can be categorized into two main categories: *i)* UAV-aided networks, where UAVs act as flying base stations, or relays, and *ii)* cellular connected unmanned aerial vehicles (CCUAVs), where UAVs connect to the network as flying user equipment (UE). In both categories, supporting UAVs with a reliable connection is essential for safe and effective operation. Cellular network connectivity provides a promising solution to this challenge, allowing UAVs to communicate with ground control stations over long distances beyond visual line of sight (BVLoS).

This research was supported by the Generalitat Valenciana, Spain, through the CIDEGENT PlaGenT, Grant CIDEXG/2022/17, Project iTENTE, and by the Spanish State Research Agency through grant PID2021-123999OB-I00 and the "Ramón y Cajal" program.

Given a fourth and/or fifth generation (4G/5G) cellular network, to provide a minimum quality of services (QoS) with reliability guarantees, e.g., 100 kbps rate and 50 ms latency at 3 nines of reliability for the command and control (C&C) channel of a CCUAV [4], most of the research has focused on the optimization of the trajectory of the CCUAV [5]–[7].

Despite the importance of UAV trajectory optimization, to support the significant growth and expansion of UAV applications, authorities and industries are working towards the creation of an organised system of UAV highways in the sky to facilitate operation management and ensure reliable connectivity on predetermined aerial routes planned according to government and/or business criteria [8], [9]. Thus, optimizing 4G, 5G networks to support a minimum QoS with reliability guarantees over a limited segregated airspace may be a more feasible and practical approach than route optimization over a given network.

The research community has begun to adopt such a complementary approach. However, only a few pioneering works exist in the literature. In [10], the authors carried out a mathematical analysis of the received signal strength (RSS) perceived by CCUAVs flying on aerial corridors, while being served by a ground cellular network. In [11], the authors explored the deployment of a new set of base stations with uptilted antennas to specifically serve aerial highways. They also propose an enhanced inter-cell interference coordination (eICIC) technique to mitigate interference to/from the aerial corridors. Similarly, in [12], the authors proposed a framework to optimize the deployment of uptilted millimetre wave (mmWave) access points to serve CCUAVs on aerial highways. In our previous work [13], instead of deploying new base stations for CCUAVs, we developed a stochastic ADAM-based optimization algorithm to fine-tune the downtilt of an existing 4G macrocellular network to maximize the CCUAV and ground UE rates, while providing a minimum SINR performance on the predefined aerial highways.

In recent years, various other solutions based on, e.g., null steering, device to device (D2D) communications, have been investigated to ensure a CCUAV reliable connectivity provided a cellular network [14]–[16]. However, none of the mentioned frameworks have investigated the importance of CCUAV cell association to the ground macrocellular network. Given that multiple CCUAVs will be closely located over the aerial highway, selecting the serving cell that provides the largest reference signal received power (RSRP) may be suboptimal

as it may not allow to efficiently exploit massive multiple-input multiple-output (mMIMO) multiplexing capabilities. In this paper, we investigate a new metric to drive the CCUAV cell association process to a mMIMO 5G network. Our proposed methodology uses planning information collected across the aerial highway to extrapolate the mMIMO multiplexing capabilities of a cell over a given route. This information, in addition to the RSRP, is then incorporated into the CCUAV cell selection logic to select the best server among the suitable set of candidates.

The rest of the paper is organized as follows. In Section II, we introduce the adopted system model. In Section III, we define the investigated cell selection metric for CCUAVs. In Section IV, we discuss our experiments and results, and finally, in Section V, the conclusions are drawn.

II. System Model

To illustrate the main concept behind the proposed metric, we consider a sub-6GHz downlink scenario comprised of $N_{\text{MS}} = 3$ macrocellular sectors covering an area of A km^2. Each sector operates at carrier frequency f_c, and is equipped with a planar mMIMO antenna panel with M active antennas, located at a height of $h_s = 25$ m. To provide more detail, the mMIMO antenna panel is composed of M_h antennas on the horizontal axis and M_v on the vertical one, i.e., $M = M_h \times M_v$. The distance between each antenna element is $\lambda_p/2$, where λ_p is the design wavelength. The mMIMO antenna panel is directed toward the center of the mentioned covered area. The total transmit power of each sector and the transmit power allocated to each physical resource block (PRB) by each sector are equal to $P_{T_x}^{\text{Tot}}$ and P_{T_x}, respectively. Note that in this paper, we consider that the total transmit power $P_{T_x}^{\text{Tot}}$ of the sector is equally divided among the N_{PRB} PRBs managed by the sector, i.e., $P_{T_x} = P_{T_x}^{\text{Tot}}/N_{\text{PRB}}$.

A set of R highways of length L_r are deployed at the center of the scenario at an altitude h_a. Such highways share the same center point, and are symmetrically rotated from each other by an angle Δ_ϕ. Each highway is defined by N_w equidistant aerial waypoints (i.e., reference points), with an inter-waypoint distance $d_w = 1$ m.

N_{ccuav} single-antenna CCUAVs are then deployed on the aerial waypoints of each highway. Following the recommendations in [17], the chosen inter-CCUAV distance is $d_{\text{ccuav}} = 50$ m. In addition to the CCUAVs, N_g single-antenna ground user equipment (gUE) are also randomly deployed within the coverage area of each sector. Figure 1 depicts the network layout and the deployed aerial highways with CCUAVs positioned on one of them.

For the sake of clarity, let us denote by $\mathbb{B}$ the set of sectors, with $\text{Card}\{\mathbb{B}\} = N_{\text{MS}}$, and by $\mathbb{D}$, $\mathbb{G}$ and $\mathbb{U}$ the sets of CCUAVs, gUEs and all UEs in the network, respectively, such that $\text{Card}\{\mathbb{D}\} = N_{\text{ccuav}}$, $\text{Card}\{\mathbb{G}\} = N_g$ and $\text{Card}\{\mathbb{U}\} = N_{\text{ccuav}} + N_g$, respectively.

For the sake of simplicity, let us assume that a sector multiplexes all its connected gUEs and CCUAVs across its bandwidth —all its PRBs.

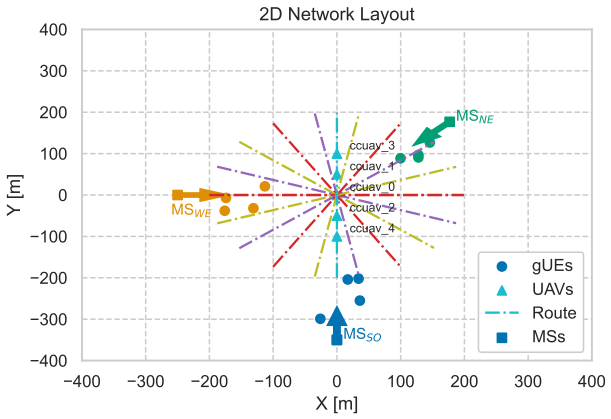

Fig. 1: 2D Network Layout with 3 MS with N_g gUEs each, R routes and N_{ccuav} CCUAVs positioned on the horizontal lane.

A. Channel Model

The large-scale channel characteristics, line of sight (LoS) probability, path loss, and shadow fading, for gUEs and CCUAVs are modelled according to the 3rd Generation Partnership Project (3GPP) urban macro scenarios in [18] and [4], respectively. We also integrate 2D spatial correlation features for the stochastic lognormal shadowing between UEs and sectors. To compute such realizations, we adopt the sum of sinusoids approach presented in [19].

The complex channel, $\mathbf{h}_{u,b} \in \mathbb{C}^{1XM}$, between a UE $u \in \mathbb{U}$ and the M antennas of the mMIMO panel of sector $b \in \mathbb{B}$ is modeled as a Rician random variable, i.e.,

$$\mathbf{h}_{u,b} = \sqrt{\frac{K}{1+K}}\,\mathbf{h}_{u,b}^{\text{LOS}} + \sqrt{\frac{1}{1+K}}\,\mathbf{h}_{u,b}^{\text{NLOS}}, \tag{1}$$

with

$$\mathbf{h}_{u,b}^{\text{LOS}} = e^{j\frac{2\pi}{\lambda_c}\mathbf{d}_{u,b}}, \tag{2}$$

and

$$\mathbf{h}_{u,b}^{\text{NLOS}} \sim \mathbb{CN}^{M}(0,1)\ , \tag{3}$$

where $\mathbf{d}_{u,b} = \left[d_{u,b}^0, \ldots, d_{u,b}^M\right]$ is the distance between a UE u and an antenna element m of the mMIMO panel of sector b, and K is the K-Rician factor, whose value is specified in [4].

B. Signal quality model

The signal y_u received at UE u from its serving sector s is formulated as

$$\begin{aligned} y_u = \sqrt{\beta_{u,s}}\,\mathbf{h}_{u,s}^H\mathbf{w}_{u,s} + \\ \sqrt{\beta_{u,s}} \sum_{p\in\mathbb{U}_s\setminus u} \mathbf{h}_{u,s}^H\mathbf{w}_{p,s} + \\ \sum_{b\in\mathbb{B}\setminus s} \sqrt{\beta_{u,b}} \sum_{i\in\mathbb{U}_b} \mathbf{h}_{u,b}^H\mathbf{w}_{i,b} + n_u\ , \end{aligned} \tag{4}$$

with

$$\beta_{u,b} = P_{T_x}\,G_{u,b}\,\rho_{u,b}\,\tau_{u,b}\ , \tag{5}$$

where $\mathbb{U}_b \subset \mathbb{U}$ is the set of UEs connected to sector b, $s \in \mathbb{B}$ is the serving sector of UE u, $G_{u,b}$, $\rho_{u,b}$ and $\tau_{u,b}$ are the

antenna, path and shadow fading gains between UE u and sector b, respectively, $\mathbf{w}_{u,b} \in \mathbb{C}^{M\times 1}$ is the precoding vector devised to serve UE u at sector b, and n_u is the thermal noise.

At a given sector b, and for a given channel matrix $\mathbf{H}_b = \left[\mathbf{h}_{1,b}, \mathbf{h}_{2,b}, \ldots, \mathbf{h}_{N_b^{\text{in}},b}\right]^T$, the precoding matrix $\mathbf{W}_b = \left[\mathbf{w}_{1,b}, \mathbf{w}_{2,b}, \ldots, \mathbf{h}_{N_b^{\text{in}},b}\right]$ is derived using zero forcing (ZF) as [14]

$$\mathbf{W}_b = \hat{\mathbf{H}}_b^H \left(\hat{\mathbf{H}}_b \, \hat{\mathbf{H}}_b^H\right)^{-1} \mathbf{D}_b^{-1/2}, \tag{6}$$

where N_b^{in} is the cardinality of set $\mathbb{U}_b$ (i.e., the number of UEs served by sector b), $\hat{\mathbf{H}}_b$ is the estimated channel matrix, and $\mathbf{D}_b^{-1/2}$ is the diagonal normalization matrix defined to satisfy the transmit power constraints, with an equal transmit power allocation for each UE in this case.

In this work, we assume that the set of pilot signals used for channel estimation at each sector is orthogonal with respect to those used at the other 2 sectors. This results in perfect channel state information (CSI), and thus the estimated and the real channel matrices coincide perfectly, i.e., $\hat{\mathbf{H}}_b = \mathbf{H}_b$.

Finally, the resulting signal-to-interference-plus-noise ratio (SINR) at UE u when associated to sector s is defined as

$$\gamma_u = \frac{P_u}{I_u + N_u} = \frac{P_u}{(I_u^{\text{intra}} + I_u^{\text{inter}}) + N_u}, \tag{7}$$

with

$$P_u = \beta_{u,s} \left|\mathbf{h}_{u,s}^H \mathbf{w}_{u,s}\right|^2, \tag{8}$$

and

$$I_u = I_u^{\text{intra}} + I_u^{\text{inter}} = \tag{9}$$
$$\sqrt{\beta_{u,s}} \sum_{p\in\mathbb{U}_s\setminus u} \left|\mathbf{h}_{u,s}^H \mathbf{w}_{p,s}\right|^2 + \sum_{b\in\mathbb{B}\setminus s} \sqrt{\beta_{u,b}} \sum_{i\in\mathbb{U}_b} \left|\mathbf{h}_{u,b}^H \mathbf{w}_{i,b}\right|^2,$$

where P_u is the useful received power at UE u, I_u is the total interference composed of the intra-cell interference I_u^{intra} and the inter-cell interference I_u^{inter}, whereas N_u is the thermal noise power. Note that, when using ZF and under perfect CSI, $I_u^{\text{intra}} = 0$ if $N_b^{\text{in}} \leq M$.

III. Serving Sector Association

In traditional cellular networks, the serving sector of each UE is typically determined using metrics related to RSRP. However, when considering CCUAVs operating at altitudes above 100 m, most of them are likely to be in LoS with many sectors, resulting in a high probability of measuring a comparable RSRP from all of them [4]. This leads to two major drawbacks: *i)* frequent handovers and ping-pong effects, and *ii)* poor experienced SINRs, driven by the high inter-cell interference. Importantly, it should be noted that when employing ZF precoding with closely-located CCUAVs, the high correlation between the complex channels of nearby CCUAVs can also lead to a noise-enhancement problem, arising from the increased values in the normalization matrix $\mathbf{D}_b^{-1/2}$, which decreases the useful received power P_u. This further affects CCUAVs performance.

In addition to the advantage of using aerial highways to manage aerial operations, knowing the a priori flight route allows extrapolating useful information on the angle of arrivals (AoAs) of CCUAVs, which can help to alleviate some of the above challenges. In the following, we concentrate on a solution for the following drawback. In conventional cellular networks, CCUAVs typically connect to the sector that provides the strongest RSRP. However, the independent design of the aerial trajectory with respect to the existing cellular network may result in scenarios where the strongest sector is unable to resolve the mMIMO spatially multiplexed communications to/from CCUAVs flying on such route and seen at approximately the same AoA. Such channel correlation would result in the mentioned noise-enhancement problem, and consequently poor overall CCUAVs SINR performance. An example of such scenario would be that where the aerial route is perpendicular to the mMIMO antenna panel of the strongest sector. In those cases, it may be beneficial to associate to a reasonably weaker sector but with better multiplexing capabilities. This is a trade-off exacerbated by the nature of aerial highways, which has never been investigated in the CCUAVs literature. To address the aforementioned issues, this study proposes a novel indicator that relies on the exploitation of predefined aerial highways design information to assign a multiplexing capability score to each sector, which can be used to drive a smarter cell selection process for CCUAVs.

A. Eigenscore-based Indicator

In this section, we introduce a new cell selection indicator for enhancing the cell selection —and thus the performance— of CCUAVs flying on aerial highways. For the sake of argument, let us consider a route r with its N_w equidistant aerial waypoints, as mentioned earlier.

In a planing stage, a complex channel vector $\mathbf{h}_{w,b}$ between each waypoint w and sector b can be calculated by performing a set of measurements, before starting to operate the aerial route, and/or using eq. (1) in this case. Then, the complex channel vectors $\mathbf{h}_{w,b}$ collected across all waypoints can be used to create the complex channel matrix $\mathbf{H}_{r,b} \in \mathbb{C}^{N_w\times M}$ associated with route r and sector b. Once the complex channel matrix $\mathbf{H}_{r,b}$ is derived for each route r and sector b, the related set of eigenvalues $\mathbf{\Lambda}_{r,b}^{\text{eig}}$ can be calculated using, e.g., single value decomposition (SVD), and scaled in the range $[0, 1]$ to proportionally identify the most relevant ones as follows

$$\bar{\mathbf{\Lambda}}_{r,b}^{\text{eig}} = \frac{\mathbf{\Lambda}^{\text{eig}}}{\sum_{\lambda_i\in\mathbf{\Lambda}_{r,b}^{\text{eig}}} |\lambda_i|^2}. \tag{10}$$

With this, we can define an eigenscore $\text{ES}_{r,b}$ for each route r and sector b as the number of eigenvalues greater than a threshold $\lambda_{\text{Th}} \in [0, 1]$, i.e.,

$$\text{ES}_{r,b} = \text{Card}\left\{\mathbb{K}_{r,b}\right\}, \text{with } \mathbb{K}_{r,b} = \left\{k \in \bar{\mathbf{\Lambda}}_{r,b}^{\text{eig}} \,|\, k \geq \lambda_{\text{Th}}\right\}. \tag{11}$$

It is worth highlighting that the defined eigenscore $\text{ES}_{r,b}$ is highly dependent on the geometry of the problem, e.g., the angle of the aerial highway with respect to the mMIMO

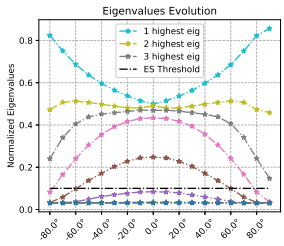

(a) Eigenvalues south ($\mathrm{MS_{SO}}$).

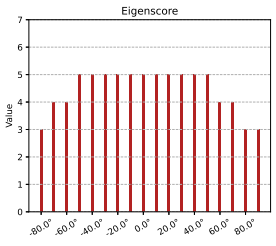

(b) Eigenscore south ($\mathrm{MS_{SO}}$).

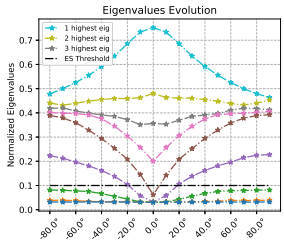

(c) Eigenvalues west ($\mathrm{MS_{WE}}$).

(d) Eigenscore west ($\mathrm{MS_{WE}}$).

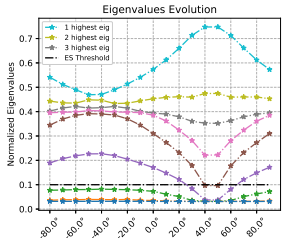

(e) Eigenvalues north-east ($\mathrm{MS_{NE}}$).

(f) Eigenscore north-east ($\mathrm{MS_{NE}}$).

Fig. 2: Eigenvalues and Eigenscore computed in each sector for different rotation or aerial highways. With threshold $\lambda_{\mathrm{Th}} = 0.10$.

antenna panel. For instance, a route r precisely aligned with the normal direction of the mMIMO antenna panel of sector b and located at the same altitude, will yield the eigenscore $\mathrm{ES}_{r,b} = 1$. Conversely, a route r parallel to the mMIMO antenna panel of sector b is likely to exhibit a higher eigenscore, i.e., $\mathrm{ES}_{r,b} > 1$ as the incoming signals are perceived with distinct AoAs. Plainly speaking, this eigenscore allows to assess the degrees of freedom that sector b has on route r. To corroborate such statements, Figure 2 illustrates, for each sector b in our network, the eigenvalues and eigenscores when assessing various routes with different orientations at an altitude of 100 m.

In this work, we are interested in considering both the signal strength and spatial diversity features of the complex channel to drive the cell selection process, with minimal changes to the state-of-the-art process. In the following, we show how this new indicator blends with the traditional RSRP-based one.

B. Enhanced Cell Selection Metric

We now exploit our proposed eigenscore $\mathrm{ES}_{r,b}$ in eq. (11) to formulate two new metrics to drive the CCUAVs cell selection process. Let us assume that, in the operational stage, each sector b broadcasts for each route r the earlier calculated eigenscore $\mathrm{ES_{r,b}}$ during the planning stage in its broadcast channel. In addition, let us assume that all CCUAVs are aware of a maximum $\mathrm{RSRP}^{\max}$ and a minimum $\mathrm{RSRP}^{\min}$ RSRP value for normalization purposes. The sector b with the resulting larger metric will be selected as server.

With this in mind, and dropping the route index r for convenience, we first define a metric $\mathbf{Z}_d^{\mathrm{SUM}}$ based on the weighted sum of the eigenscore of each sector b and the RSRPs of each CCUAVs d, as follows

$$\mathbf{Z}_d^{\mathrm{SUM}} = \alpha \frac{\mathbf{ES} - \mathrm{ES}^{\max}}{\mathrm{ES}^{\max} - \mathrm{ES}^{\min}} + \\ + (1-\alpha)\frac{\mathbf{RSRP}_d - \mathrm{RSRP}^{\max}}{\mathrm{RSRP}^{\max} - \mathrm{RSRP}^{\min}}, \tag{M1}$$

where α is a weighting factor, $\mathbf{ES} = [\mathrm{ES}_1, \ldots, \mathrm{ES}_{N_{\mathrm{MS}}}]$ is the vector containing the eigenscores broadcasted by each sector b, $\mathbf{RSRP}_d = [\mathrm{RSRP}_1, \ldots, \mathrm{RSRP}_{N_{\mathrm{MS}}}]$ is the vector containing the RSRPs of CCUAV d with respect to each sector b, $\mathrm{ES}^{\max} = \max(\mathbf{ES})$ and $\mathrm{ES}^{\min} = \min(\mathbf{ES})$. Intuitively, the objective of this metric is to consider the eigenscore as a power offset to the traditional RSRP-based metric during the cell selection process. This would facilitate the computations at the CCUAV, as the eigenscore, as mentioned earlier, can be broadcast by each sector in their control channels, e.g., physical broadcast channel (PBCH).

The second defined metric $\mathbf{Z}_d^{\mathrm{CAP}}$ based on the proposed eigenscore is inspired by the Shannon–Hartley channel capacity theorem, and has been formulated as follow

$$\mathbf{Z}_d^{\mathrm{CAP}} = \mathbf{ES}\log_2(1 + \mathbf{SNR}_d) \sim \\ \sim \mathbf{ES}\log_2(1 + \mathbf{RSRP}_d). \tag{M2}$$

This metric attempts to assess the achievable capacity of CCUAV d in a noise-limited regime, taking into account the multiplexing capabilities of the sector on the route and the signal strength measured by the CCUAV. The computation of this metric is more involved than the previous one, but allows to capture the linear and logarithmic relationship between spatial multiplexing and signal strength in terms of capacity. No normalisation is needed.

IV. Evaluation and Discussion

In this section, we evaluate the performance achieved by our proposed metrics when adopted to drive the cell selection process of CCUAVs. We adopt the scenario presented in Section II. Note that $N_{\mathrm{ccuav}} = 5$ CCUAVs are deployed on each aerial highway. The values of other parameters adopted in the numerical analysis are reported in Table I. Note that due to space constraints, we discuss the results obtained over a single aerial route, that with $\Delta_\phi = 90°$. However, similar results were obtained for all routes.

A. Cell Selection Rate

In this section, we analyse the impact of the selected cell selection metric on the cell selection rate, defined as the probability that an arbitrary CCUAV selects a given sector as a serving one.

Figure 3 shows the cell selection rate of the 5 deployed CCUAVs when considering three metrics: M1, M2, and RSRP.

TABLE I: Summary of the parameters used.

Param	Value	Param	Value
A	0.22 Km^2	N_{MS}	3
M	64	M_h, M_v	4,4
λ_p	8.57 cm	f_c	3.5 GHz
N_g	4	L_r	400 m
R	18	N_w	400
Δ_ϕ	10°	h_a	1.5 m
d_{ccuav}	50 m	h_a	100 m
N_{ccuav}	$\{1,\ldots,7\}$	N_{Drop}	1000
N_{PRB}	100	$P_{T_x}^{\text{Tot}}$	46 dBm
P_{T_x}	26 dBm	K	14.22 dB
λ_{Th}	0.10	α	0.50

The first two metrics are the proposed ones, and the last one, noted as RSRP, is the metric typically used in traditional networks, which is used here as a benchmark.

As shown in Figure 3(a), when using the RSRP metric, some of the CCUAVs tend to associate to the south sector MS_{SO}, as it provides the strongest RSRP. For instance, ccuav_4 connects 67.10% of the time to the south sector MS_{SO}. When considering the other two studied metrics M1 and M2, such rates dramatically change to 0.00% and 18.60%, respectively. Even if the south sector, MS_{SO}, may provide the largest received power, the new eigenscore-based metrics lead to associations with sectors possessing better spatial resolution capabilities, i.e., MS_{WE} and MS_{NE}, as their mMIMO panels have a better geometry with respect to the route, As shown in Figure 2, for the selected route, note that the south sector MS_{SO} has the worst eigenscore, meaning that it cannot discern as many AoAs on the route as the other two sectors MS_{WE} and MS_{NE}. Thus, associating more CCUAVs with the former sector leads to reduced spatial resolution, and ultimately reduced performance, as demonstrated in the following section.

It is worth highlighting that the results of this study also suggest that the two proposed metrics can be leveraged to reduce the number of candidate serving sectors for CCUAVs, resulting in fewer handovers and improved network stability. This can help to reduce overhead and handover failures, and thus enhance performance of the network.

B. SINR Performance

In the following, we analyse the UE SINR performance to further highlight the benefits of the proposed metrics when adopted to drive the CCUAV cell selection process.

Figure 4 shows the SINR distribution of the 5 deployed CCUAVs when considering the three metrics discussed earlier: M1, M2, and RSRP.

The results show that when the proposed eigenscore-based metrics are adopted for driving the cell selection process, an important increase in both average and 5%-tile SINRs is achieved. Specifically, metric M1 achieves a gain of 3.30 dB and 3.13 dB with respect to the RSRP metric at the average and 5%-tile SINRs, respectively, while the respective gains of metric M2 are 2.36 dB and 1.66 dB. A summary of the CCUAV SINRs and gains can be found in Table II.

To further analyse the benefits of such metrics to support the reliable connectivity of multiple closely located CCUAVs, Figure 5 shows how the 5%-tile SINR evolves when more

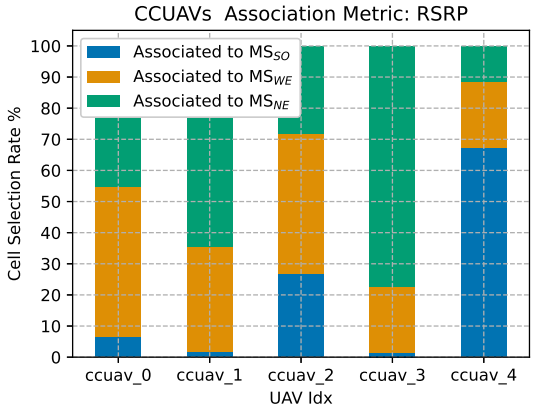

(a) Cell selection rates using RSRP metric.

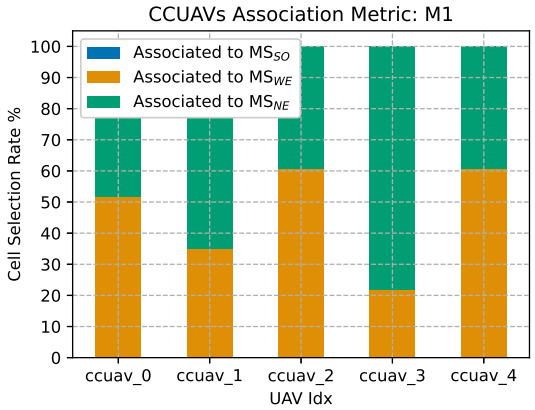

(b) Cell selection rates with summation based metric eq. (M1).

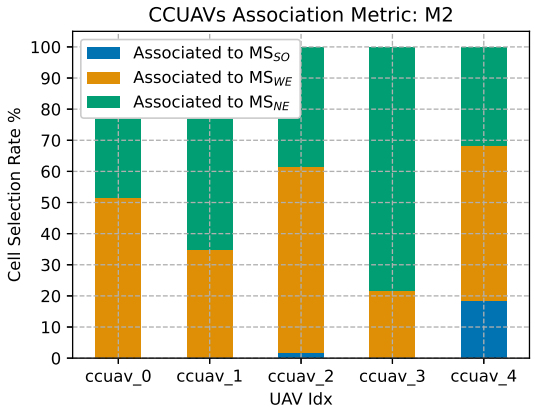

(c) Cell selection rates with capacity based metric eq. (M2).

Fig. 3: Cell selection rates of 5 CCUAVs on the vertical aerial highway (i.e., route rotated by 90°).

and more CCUAVs fly on the same aerial highway (up to 7 CCUAVs with an inter-CCUAV distance of $d_{\text{ccuav}} = 50$ m). The results show that using the proposed metrics results in a significantly improved 5%-tile SINR when compared to the RSRP metric. Metrics M2 and M1 achieve a maximum gain of 3.70 dB and 4.18 dB for the case with 3 CCUAVs and 7 CCUAVs, respectively. A summary of the CCUAV 5%-tile SINR and respective gains can be found in Table III.

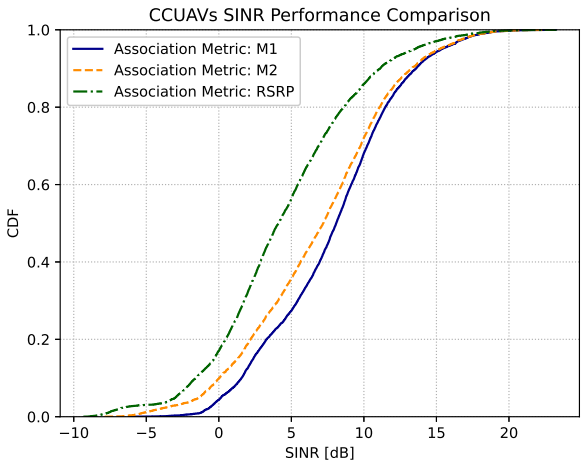

Fig. 4: SINR comparison of CCUAVs placed on the vertical route.

TABLE II: Summary of SINR results for different association metric.

	Association Metric		
	M1	**M2**	**RSRP**
Aerial 5%-tile SINR [dB]	0.16	-1.31	-2.97
Gain 5%-tile to RSRP [dB]	3.13	1.66	–
Aerial mean SINR [dB]	7.79	6.85	4.49
Gain to RSRP [dB]	3.30	2.36	–

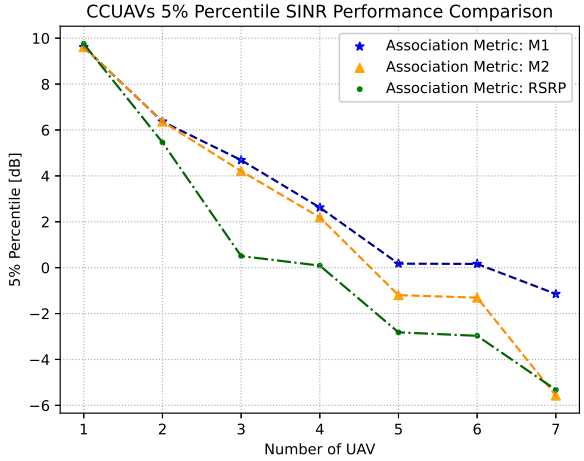

Fig. 5: 5%-tile SINR versus the number of CCUAVs.

TABLE III: Summary of 5%-tile SINR results for different association metric and number of CCUAVs.

	Number of CCUAVs						
Metric	**1**	**2**	**3**	**4**	**5**	**6**	**7**
M1 [dB]	9.61	6.37	4.69	2.62	0.17	0.16	-1.14
M2 [dB]	9.61	6.37	4.21	2.19	-1.20	-1.31	-5.57
RSRP [dB]	9.76	5.46	0.09	0.09	-2.82	-2.97	-5.32
Gain M1-RSRP [dB]	-0.14	0.91	2.53	2.53	2.99	3.13	4.18
Gain M2-RSRP [dB]	-0.14	0.91	2.10	2.10	1.62	1.66	-0.25

In summary, the improved performance when using the proposed metrics can be attributed to two factors. Firstly, the eigenscore enables the identification of cells that are more capable of effectively resolving AoAs, resulting in a higher multiplexing gain with mMIMO. Secondly, narrowing the pool of serving cell candidates reduces inter-cell interference.

The results show that using RSRP as the sole metric for choosing the serving cell among multiple suitable candidates is not the optimal solution. Integrating our proposed eigenscore into the cell association metric allows for better and fairer SINR performance in mMIMO-based networks. In our results, using metric M1 instead of M2 yields better results. This suggests to network operators, which plan to integrate aerial highway systems into their network, that they should incorporate such an eigenscore as an offset value to drive their cell selection and potentially handover processes. Further studies are needed.

V. Conclusion

In this paper, we have proposed a novel metric to drive the cell selection process of UAVs on aerial highways supported by a terrestrial mMIMO network. Our results showed that integrating our proposed metric, which is capable of capturing information on the spatial diversity between each aerial highway and sector, allows recognising and then associating with serving cells that provide a better and fairer SINR performance, especially when the number of flying CCUAVs increases. Future work will enhance our considerations, by extending the metric also to embrace additional features such as information on the ground traffic condition.

References

[1] Y. Zeng *et al.*, *UAV Communications for 5G and Beyond*. Wiley, 2020.

[2] G. Geraci et al., "What will the future of UAV cellular communications be? A flight from 5G to 6G," *IEEE Commun. Surveys & Tutorials*, vol. 24, no. 3, pp. 1304–1335, 2022.

[3] A. Jonas et al., *"eVTOL/Urban Air Mobility TAM Update: A Slow Take-Off, But Sky's the Limit"*. Morgan Stanley Research, 2021.

[4] 3GPP TR 36.777, "Enhanced LTE support for aerial vehicles," Jan. 2017.

[5] N. Cherif *et al.*, "Disconnectivity-aware energy-efficient cargo-UAV trajectory planning with minimum handoffs," in *Proc. IEEE ICC*, 2021.

[6] O. Esrafilian *et al.*, "3D-map assisted UAV trajectory design under cellular connectivity constraints," in *Proc. IEEE ICC*, 2020, pp. 1–6.

[7] U. Challita *et al.*, "Deep reinforcement learning for interference-aware path planning of cellular-connected UAVs," in *Proc. IEEE ICC*, 2018, pp. 1–6.

[8] F.A.A., *Pilot's Handbook of Aeronautical knowledge*. U.S. Department of Transportation, 2016.

[9] N. Cherif *et al.*, "3D aerial highway: The key enabler of the retail industry transformation," *IEEE Commun. Mag.*, vol. 59, no. 9, pp. 65–71, 2021.

[10] S. Karimi-Bidhendi *et al.*, "Analysis of UAV corridors in cellular networks," in *Proc. IEEE ICC*, 2023, pp. 1–6.

[11] M. M. U. Chowdhury *et al.*, "Ensuring reliable connectivity to cellular-connected UAVs with up-tilted antennas and interference coordination," *ITU J. Future and Evolving Technol.*, 2021.

[12] S. Singh *et al.*, "Placement of mmWave base stations for serving urban drone corridors," in *Proc. IEEE VTC-Spring*, 2021, pp. 1–6.

[13] M. Bernabè *et al.*, "On the optimization of cellular networks for UAV aerial corridor support," in *Proc. IEEE Globecom*, 2022, pp. 2969–2974.

[14] G. Geraci *et al.*, "Understanding UAV cellular communications: From existing networks to massive MIMO," *IEEE Access*, vol. 6, 2018.

[15] S. Kang *et al.*, "Coexistence of UAVs and terrestrial users in millimeter-wave urban networks," in *Proc. IEEE Globecom Workshops*, 2022, pp. 1158–1163.

[16] M. Benzaghta *et al.*, "UAV communications in integrated terrestrial and non-terrestrial networks," in *Proc. IEEE Globecom*, 2022, pp. 3706–3711.

[17] E. Vinogradov and S. Pollin, "Reducing safe UAV separation distances with U2U communication and new remote ID formats," in *Proc. IEEE Globecom Workshops*, 2022, pp. 1–6.

[18] 3GPP TR 38.901, "Study on channel model for frequencies from 0.5 to 100 GHz," Mar. 2017, v. 14.0.0.

[19] X. Cai and G. Giannakis, "A two-dimensional channel simulation model for shadowing processes," *IEEE Trans. on Vehicular Tech.*, vol. 52, no. 6, pp. 1558–1567, 2003.